BIOCHEMISTRY
including biophysical chemistry & molecular biology

Article

pubs.acs.org/biochemistry

Structure and Mechanism of PhnP, a Phosphodiesterase of the Carbon-Phosphorus Lyase Pathway

Shu-Mei He,[†] Matthew Wathier,[†] Kateryna Podzelinska,[‡] Matthew Wong,[†] Fern R. McSorley,[†] Alemayehu Asfaw,[†] Bjarne Hove-Jensen,[§] Zongchao Jia,[‡] and David L. Zechel*[,†]

[†]Department of Chemistry and [‡]Department of Biochemistry, Queen's University, Kingston, Ontario K7L 3N6, Canada
[§]Department of Biology, University of Copenhagen, DK-2200 Copenhagen N, Denmark

Supporting Information

ABSTRACT: PhnP is a phosphodiesterase that plays an important role within the bacterial carbon-phosphorus lyase (CP-lyase) pathway by recycling a "dead-end" intermediate, 5-phospho-α-D-ribosyl 1,2-cyclic phosphate, that is formed during organophosphonate catabolism. As a member of the metallo-β-lactamase superfamily, PhnP is most homologous in sequence and structure to tRNase Z phosphodiesterases. X-ray structural analysis of PhnP complexed with orthovanadate to 1.5 Å resolution revealed this inhibitor bound in a tetrahedral geometry by the two catalytic manganese ions and the putative general acid residue H200. Guided by this structure, we probed the contributions of first- and second-sphere active site residues to catalysis and metal ion binding by site-directed mutagenesis, kinetic analysis, and ICP-MS. Alteration of H200 to alanine resulted in a 6−33-fold decrease in k_{cat}/K_M with substituted methyl phenylphosphate diesters with leaving group pK_a values ranging from 4 to 8.4. With bis(*p*-nitrophenyl)phosphate as a substrate, there was a 10-fold decrease in k_{cat}/K_M, primarily the result of a large increase in K_M. Moreover, the nickel ion-activated H200A PhnP displayed a bell-shaped pH dependence for k_{cat}/K_M with pK_a values (pK_{a1} = 6.3; pK_{a2} = 7.8) that were comparable to those of the wild-type enzyme (pK_{a1} = 6.5; pK_{a2} = 7.8). Such modest effects are counter to what is expected for a general acid catalyst and suggest an alternate role for H200 in this enzyme. A Brønsted analysis of the PhnP reaction with a series of substituted phenyl methyl phosphate esters yielded a linear correlation, a β_{lg} of −1.06 ± 0.1, and a Leffler α value of 0.61, consistent with a synchronous transition state for phosphoryl transfer. On the basis of these data, we propose a mechanism for PhnP.

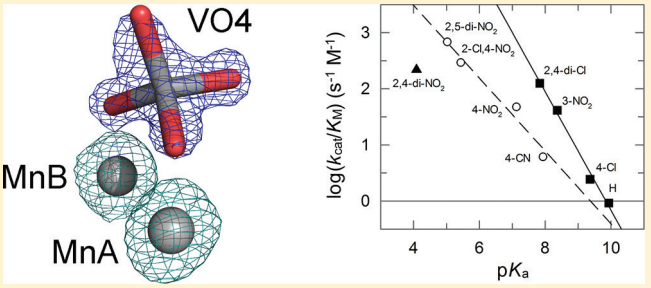

The catabolism of organophosphonates by *Escherichia coli* is performed by a set of 14 proteins encoded by the *phn* operon (*phnCDEFGHIJKLMNOP*).[1−3] A critical step in this process is cleavage of the carbon−phosphorus (CP) bond, yielding a hydrocarbon and an unknown phosphorus-containing compound.[4] This is an unprecedented enzyme reaction and particularly astonishing considering the chemical stability of the CP bond. Because the CP bond cleaving activity of *E. coli* was discovered decades prior to the characterization of the encoding *phn* operon,[5] the name CP-lyase arose to collectively describe what is now known to be a multienzyme system.[6] It is also known that naturally occurring organophosphonate levels often exceed inorganic phosphate levels in the environment, and thus, expression of the *phn* operon provides bacteria with a selective advantage in phosphate poor conditions.[7,8] For this reason, it is not surprising that the *phn* operon is widely distributed in bacterial species.[9] At present, it is known that *phnCDE* encode an organophosphonate transport system,[10,11] with PhnD acting as a periplasmic organophosphonate binding protein,[12] and that *phnF* likely encodes a repressor of the *phn* operon based on sequence homology of PhnF to *Mycobacterium smegmatis* PhnF.[13] The CP bond cleavage step, which is proposed to proceed through a radical mechanism,[14−16] may be encoded by *phnGHIJKLM*.[17,18] The surprising number of genes encoding what is nominally a single reaction step is in part explained by the formation of a soluble protein complex, PhnGHIJK,[19] in which each protein likely contributes structural and catalytic elements to a holoenzyme complex. *phnO* of *Salmonella enterica* was shown to encode an *N*-acetyltransferase that catalyzes the acetylation of aminoalkylphosphonates, including the widespread natural product 2-aminoethyl phosphonate.[20] Acetylation may be necessary for the catabolism of such compounds by CP-lyase as the corresponding acetylated aminoalkanes are detected as degradation products.[21] Finally, *phnN* encodes an ATP-dependent phosphokinase that catalyzes an equilibrium between 5-phospho-α-D-ribosyl 1-diphosphate and α-D-ribosyl 1,5-bisphosphate.[22] Recent work by our group suggests the latter compound is used to initiate each CP-lyase reaction cycle.[23]

Received: April 11, 2011
Revised: July 14, 2011
Published: August 10, 2011

Table 1. Sequences of Mutagenic Primers Used To Generate *phnP* Mutants and the Corresponding Mutagenesis Method

mutation	sequence (5′ → 3′)[a]	mutagenesis method
H78A	TTGCTGACGCATTATGCGATGGATCACGTCCAG	QuikChange
T75A	CCAGCAGTTTTTGCTGGCGCATTATCATATGGATC	QuikChange
D164A	GTGGCGTGGCTGTCTGCCACCGCAGGTTTGCCG	QuikChange
H200A	GATGCACCGCGTAATGCCTGTGATTTAAATACC	QuikChange
H222A	CGGGTGATTCTGACCGCGATCAGCCACCAGTTTG	QuikChange
D187A	CAGGTAATGGTGATGGCGTGCAGTCACCCGCCG	QuikChange
D54A	CGCAATCACCCTGATCGCCGCCGGGCTGCACGATC	4-primer
PhnP for	CACACAGAATTCATTAAAGAGG	4-primer
PhnP rev	GAGCCATGGTTATTAATGGTG	4-primer

[a]Mutagenic codons are underlined. Only the forward primer sequence is given. The reverse primer is the complementary sequence.

The *phnP* gene encodes a phosphodiesterase that belongs to the large and diverse metallo-β-lactamase family of hydrolases.[24,25] Initial biochemical and structural studies by our group revealed PhnP to be a dimeric enzyme possessing a dinuclear active site that is typical for this family, as well as a structural zinc ion that is conserved in PhnP homologues.[26] PhnP also exhibited specificity toward 2′,3′-cyclic nucleotides and a distinct preference for manganese and nickel ions for activity. ICP-MS analysis indicated that PhnP can be isolated from *E. coli* with substoichiometric quantities of the former metal ion. In more recent work, we discovered that the in vivo substrate for PhnP is 5-phospho-α-D-ribosyl 1,2-cyclic phosphate, which we propose is a "dead-end" intermediate generated by the CP bond cleaving step of the CP-lyase pathway.[23,27] PhnP regiospecifically converts this cyclic intermediate to α-D-ribosyl 1,5-bisphosphate, the putative initiator of the CP-lyase reaction. The PhnP active site residues are strictly conserved with other members of the metallo-β-lactamase family, including the tRNase Z phosphodiesterases[28,29] and glyoxalase II.[25] Two of these residues, H200 and D80, stand out for their proposed roles in catalysis. H200 is believed to function as a general acid for leaving group stabilization,[30,31] whereas D80 may have a more complex role, simultaneously acting as a metal ion ligand and a general base for activation of water as a nucleophile,[32] as has been proposed for metallo-β-lactamases.[33]

In this study, we examine the roles of active site residues through a combination of structural analysis of PhnP in complex with a phosphate analogue, orthovanadate, and kinetic analysis of active site variants. We have also analyzed the leaving group dependence of the PhnP reaction with a linear free energy relationship. This has allowed a more precise description of the transition-state character of the PhnP reaction and the role of active site residues in this process.

MATERIALS AND METHODS

Materials. Unless otherwise noted, all chemicals were obtained from Sigma-Aldrich. DNA primers were synthesized by Sigma-Genosys. Restriction enzymes were obtained from New England Biolabs or Fermentas. DNA sequencing was performed at the Robarts Research Institute (London, ON). Methyl phenylphosphate diesters were either obtained as generous gifts from R. S. Brown and T. Liu (Department of Chemistry, Queen's University) or synthesized as lithium salts from the corresponding phenolates and dimethyl chlorophosphate according to the literature procedure.[34] Synthesized substrates were recrystallized from acetone with methanol or tetrahydrofuran with methanol and afforded ^{1}H NMR and ^{31}P NMR spectra consistent with literature characterization (see the Supporting Information).[35]

Crystallization and X-ray Structural Analysis. Wild-type (WT) PhnP was dialyzed against 20 mM HEPES (pH 7.5) and 150 mM NaCl, concentrated to 13 mg/mL, and then flash-frozen in liquid nitrogen as 100 μL aliquots until needed. Orthovanadate was added to PhnP to a final concentration of 0.5 mM (1:2 PhnP:vanadate molar ratio), along with 50 mM L-arginine, 50 mM L-glutamate, and 0.5 mM $MnCl_2$ (pH 7.6). The resulting mixture was incubated for 1 h. A 2 μL aliquot of this solution was mixed with 2 μL of a precipitant solution, and the resulting drop was streak-seeded with a freshly crushed crystal using a horse hair. The protein was crystallized at room temperature in a sitting drop format on a microbridge containing 20 μL of Flourinert (Hampton). Optimized crystallization conditions consisted of 0.1 M 2-(*N*-morpholino)ethanesulfonic acid (MES), pH 5.2, and 7% PEG 8000. Prior to data collection, the crystals were extracted from the drop and dragged through a Fluorinert solution until all mother liquor solution was removed from the loop, after which the crystals were flash-frozen in liquid nitrogen. The native data set was recorded at 100 K at the Argonne Advanced Photon Source (Chicago, IL) at beamline GM/CA-CAT using a Mar 300 CCD detector. The data were indexed and scaled using HKL2000.[36] The structure of PhnP in complex with orthovanadate was determined by direct refinement using the apo-PhnP structure with the malate ligand removed[26] in REFMAC5.[37] The structure was further refined using Phenix[38] and visualized in Coot.[39] The final model contained a dimer in the asymmetric unit, along with 521 water molecules, four manganese ions, two zinc ions, and two orthovanadate ions. The occupancy of the metal ions was refined manually by adjusting the occupancy values until no density was observed in the residual map. A model of PhnP bound to the in vivo substrate 5-phospho-α-D-ribosyl 1,2-cyclic phosphate was obtained by manually docking an energy-minimized structure of the substrate into the active site using PyMol. Energy minimization of the substrate with the MM2 force field was performed with Chem3D Pro 12.0 (CambridgeSoft). The cyclic phosphate diester was aligned with the bound orthovanadate with an orientation appropriate for in-line attack by water to afford α-D-ribosyl 1,5-bisphosphate as the product. Structural alignment of PhnP with the *Brucella melitensis* phosphodiesterase [Proton Data Bank (PDB) entry 3md7] was performed with DaliLite.[40] The coordinates and structure factors for PhnP have been deposited as PDB entry 3P2U.

Preparation of WT PhnP and Active Site Variants. Mutagenesis of the *phnP* gene was conducted according to the QuikChange site-directed mutagenesis protocol (Stratagene) or by four-primer overlap-extension PCR using *Pfu* turbo DNA polymerase (Stratagene) and plasmid pHO520-*phnP* as a

template.[41] Mutagenic and flanking primers are listed in Table 1. In the case of four-primer overlap-extension PCR, the assembled PCR products were digested with *Eco*RI and *Bam*HI and ligated into similarly digested pUHE23-2.[41] The sequences of the desired mutant alleles were confirmed by sequencing both DNA strands. All of the *phnP* alleles specified polypeptides with hexahistidine tags at the C-termini. WT and mutant *phnP* alleles were expressed in *E. coli*, and the specified enzymes were purified by Ni-NTA chromatography as described previously.[41]

ICP-MS Analysis. The zinc and manganese ion contents of PhnP variants isolated from *E. coli* cultures grown in LB medium were determined as described previously.[26] To determine the ability of WT PhnP and mutant variants to incorporate and retain manganese ions, purified proteins in 50 mM HEPES (pH 7.5) and 150 mM NaCl were incubated with excess $MnCl_2$ (1 mM) for 3 h at 4 °C and then dialyzed twice against the buffer described above. An aliquot of the final dialysis buffer was saved for dilution of PhnP samples and ICP-MS analysis of background metal ion content. Alternatively, WT PhnP and mutant variants were synthesized in *E. coli* cultures supplemented with 500 μM $MnCl_2$ and then purified and dialyzed in the buffer described above. Manganese dichloride standard solutions (0−20 μM) were prepared using dialysis buffer. Each PhnP sample was filtered (0.22 μm) and its concentration (based on the monomer) adjusted to 10 μM with saved dialysis buffer immediately prior to analysis. The manganese ion content of each sample was measured using a Varian 820-MS ICP mass spectrometer with the following settings: plasma flow, 18.0 L min^{-1}; auxiliary flow, 1.80 L min^{-1}; nebulizer flow, 1.01 L min^{-1}; sheath gas flow, 0.15 L min^{-1}. Measurements (in triplicate) were corrected for residual metal content by analyzing the used dialysis buffer alone.

CD Spectroscopy. PhnP and mutant variants were dialyzed overnight against 10 mM Tris-HCl (pH 7.2) and concentrated to 70 μM by ultrafiltration (Millipore Amicon Ultra, 10 kDa molecular mass cutoff). CD spectra were recorded in Suprasil quartz cuvettes at 20 °C using an Applied Photophysics ChiraScan CD spectrophotometer. Five replicate spectra were averaged for each protein and smoothed using Applied Photophysics Pro-Data Suite 4.1.2.

Steady-State Kinetic Analysis of PhnP. Reactions were performed at 25 °C in 50 mM Tris-HCl (pH 7.1) and 150 mM NaCl containing 1 mg/mL BSA and 1.0 mM $MnCl_2$ unless otherwise noted. WT PhnP cannot be purified from *E. coli* in a fully metal ion-loaded form (only ∼0.1 manganese ion per active site)[26] and displays saturation kinetics with respect to manganese ion concentration with an apparent K_M value of 130 μM (data not shown). For this reason, all kinetic analyses were performed with 1 mM $MnCl_2$, which is saturating for the WT enzyme. Reactions were initiated via the addition of a concentrated aliquot of PhnP to the reaction solution (5−20 μL). The final concentration of PhnP ranged from 0.5 to 20 μM, depending on the substrate used. Initial rates were measured on a Cary Bio 300 spectrometer (Varian) over the first 5−10 min of the reaction. The wavelengths and extinction coefficients used for the measurement of the PhnP-catalyzed hydrolysis rates of substituted methyl phenylphosphate diesters or bpNPP are as follows: 400 nm and 11100 M^{-1} cm^{-1} for 2,4-dinitrophenyl, 445 nm and 4300 M^{-1} cm^{-1} for 2,5-dinitro, 400 nm and 16350 M^{-1} cm^{-1} for 2-chloro-4-nitro, 400 nm and 11034 M^{-1} cm^{-1} for 4-nitro, 290 nm and 634 M^{-1} cm^{-1} for 2,4-dichloro, 270 nm and 3101 M^{-1} cm^{-1} for 4-cyano, 380 nm and 385 M^{-1} cm^{-1} for 3-nitro, 278 nm and 580 M^{-1} cm^{-1} for 4-chloro, and 277 nm and 778 M^{-1} cm^{-1} for phenyl methylphosphate. Extinction coefficients for 4-nitro- and 2,4-dichlorophenolates were determined experimentally from a plot of absorbance versus the concentration of phenolate dissolved in the reaction buffer (pH 7.1). All other extinction coefficients and pK_a^{LG} values were previously published.[34,35,42,43] It was not possible to achieve saturation with the methyl phenylphosphate diesters (up to 10 mM substrate); therefore, k_{cat}/K_M values were determined from the slope of substrate concentration versus reaction velocity (0−5 mM substrate). For the substrate bpNPP, where saturation was observed, substrate concentrations ranged from 0.2 to 5 times the final determined K_M value. Kinetic parameters were obtained from a fit of the rate dependence on substrate concentration with the Michaelis−Menten equation using GraFit 6.0.[44] Although the WT enzyme exhibits cooperative kinetics with bpNPP,[26] this effect is weak, and therefore, application of the Michaelis−Menten equation has a minimal impact on the calculated k_{cat} and K_M values. The assays for phosphate and orthovanadate inhibition of PhnP were performed with bpNPP in 50 mM Tris-HCl (pH 7.1), 1 mM $MnCl_2$, 150 mM NaCl, and 1 mg/mL BSA, equilibrated at 25 °C. K_I values were calculated for orthovanadate by a global fit of the data to a mixed inhibition equation using GraFit 6.0. The data for phosphate inhibition were fit to a competitive inhibition equation (see the Supporting Information).

pH Dependence of PhnP Activity. The pH dependence of bpNPP hydrolysis by PhnP was conducted in solutions buffered by MES (pH 5.2−6.8), BES (pH 6.5−7.8), or Tris-HCl (pH 7.8−9). Reaction mixtures consisted of 50 mM buffer, 150 mM NaCl, 1 mg/mL BSA, 50 μM bpNPP, and either 1 mM $MnCl_2$ or 1 mM $NiCl_2$. No effects of buffer concentration on the rate of reaction of PhnP with bpNPP were observed. Residual active site metal ions were removed from the WT enzyme or H200A prior to analysis by incubation with 10 mM EDTA for 1 h followed by extensive dialysis (three buffer changes) against 50 mM Tris-HCl (pH 7.2) and 150 mM NaCl (all steps conducted at 4 °C). Reactions were initiated by the addition of 5−10 μL of metal ion free PhnP to a 750 μL reaction solution pre-equilibrated at 25 °C. The final enzyme concentrations were 5 μM WT PhnP for the $MnCl_2$ reactions, 2.5 μM WT PhnP for the $NiCl_2$ reactions, and 5 μM H200A PhnP for the $NiCl_2$ reactions. The reaction with bpNPP was followed at 400 nm for the release of *p*-nitrophenolate for three or four half-lives. It was determined that the activities of WT PhnP and H200A PhnP did not decrease more than 10% when they were incubated at each pH for the duration of these experiments. Because the concentration of bpNPP is far lower than the K_M values for WT PhnP and H200A (3 and 18 mM, respectively),[26] k_{cat}/K_M was calculated directly from a fit of the absorbance versus time data to the integrated pseudo-first-order rate equation (eq 1) using GraFit 6.0.[44]

$$\frac{A_t}{A_0} = 1 - e^{-k_{obs}E_T t} \quad (1)$$

where $k_{obs} = k_{cat}/K_M$, E_T is the total PhnP concentration, and A_0 and A_t are the absorbance values at time zero and time t, respectively. Values of k_{cat}/K_M were determined in triplicate at each pH. Finally, the pH dependence of k_{cat}/K_M was fit to eq 2 using GraFit 6.0, which describes a bell-shaped pH profile arising from two ionizable groups:

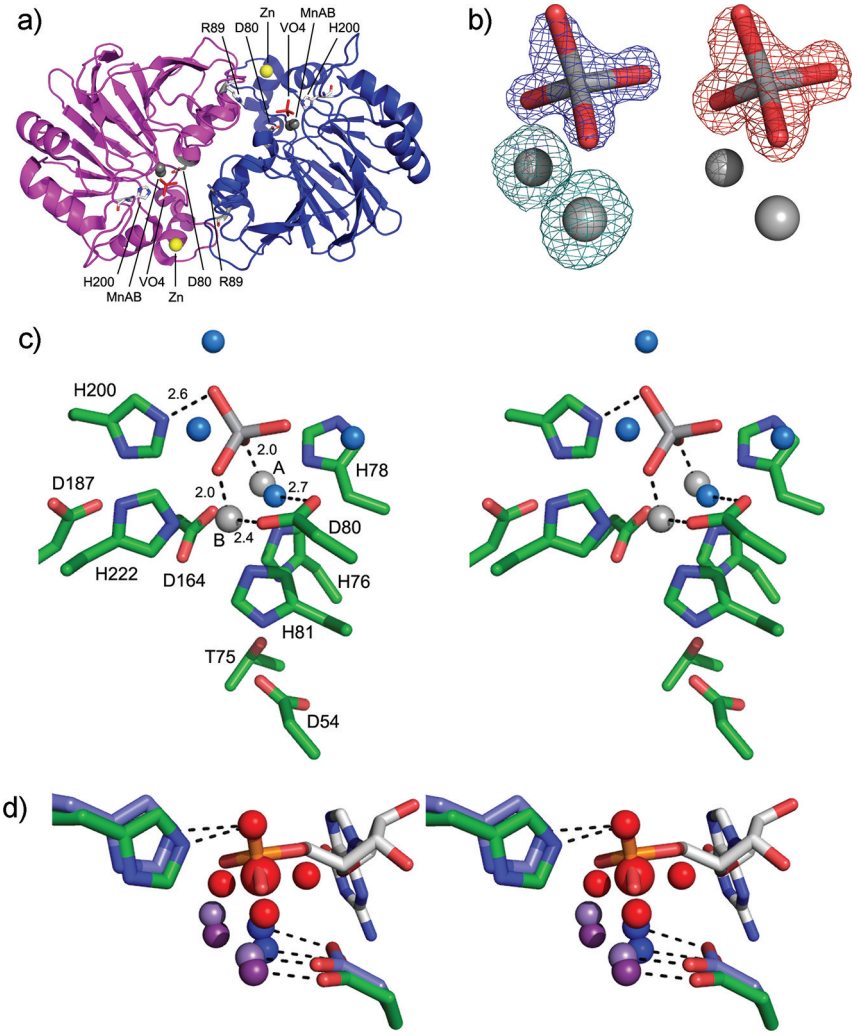

Figure 1. Structure of PhnP bound to orthovanadate. (a) PhnP dimer with subunits A and B colored magenta and blue, respectively. The structural zinc ion and active site manganese ions (MnA and MnB) are shown as yellow and gray spheres, respectively. Orthovanadate is shown as red sticks. Active site residues D80, R89, and H200 are shown as gray sticks. (b) Interactions of the orthovanadate with manganese ions (colored gray). The $2F_o - F_c$ density at the 1σ level (left) is shown as blue and teal mesh for orthovanadate and the manganese ions, respectively. The omit map for vanadate (right), contoured at the 3.5σ level, is shown as a red mesh. (c) "Wall-eyed" stereoview of the active site of PhnP bound to orthovanadate. Bound water molecules are colored blue. Orthovanadate is shown as red and gray sticks. Key interactions formed by H200, D80, and the manganese ions (MnA and MnB) are shown as dashed lines with distances in angstroms. (d) Wall-eyed stereoview of the PhnP–orthovanadate complex superimposed with *B. melitensis* phosphodiesterase (PDB entry 3md7) bound to guanosine 5′-monophosphate (gray sticks). PhnP residues D80 and H200 are colored green and *B. melitensis* enzyme residues D90 and H219 blue. The orthovanadate atoms are depicted as red spheres, and the phosphoryl group of guanosine 5′-monophosphate is shown as orange and red sticks. Manganese ions for both enzymes are shown as purple or teal spheres.

$$\left(\frac{k_{cat}}{K_M}\right)_{obs} = \frac{\left(\frac{k_{cat}}{K_M}\right)_{max} \times 10^{pH-pK_{a1}}}{10^{2\times pH-pK_{a1}-pK_{a2}} + 10^{pH-pK_{a1}} + 1} \quad (2)$$

RESULTS

PhnP–Orthovanadate Complex. The X-ray crystal structure of PhnP bound to orthovanadate was determined to 1.5 Å resolution by direct refinement with the original PhnP structure.[26] PhnP crystallized as a dimer (Figure 1a); of 258 residues per monomer, molecule A contains residues 2–250, including all the side chains, whereas molecule B contains residues 2–251. No clear density was present for the C-terminal hexahistidine tag in either of the subunits (residues 253–258). The model was refined to an *R* factor of 16.1% and an R_{free} of 18.6% (Table 2). The model possesses good geometry, where 87.2% of the residues fall in the most favored regions of the Ramachandran plot, 11.1% in additional allowed regions, and 1% in generously allowed regions. Three residues, D54, N47, and D108, fall in the disallowed regions of the plot (0.7%). N47 is a solvent-exposed residue on the surface of the protein, located in the β-hairpin between β-strands 2 and 3. This residue makes a 3.7 Å interaction with the hydroxyl of S2. Essentially identical dihedral angles of 55° (ϕ) and −119° (ψ) are observed for this residue in both monomers. D108 is located in the unstructured loop between β5 and α5, making hydrogen bonding interactions with two water molecules and D109. Dihedral angles of 47° (ϕ) and −134° (ψ) are observed for this residue in both monomers. Neither N47 nor D108 is conserved in the PhnP family or with structural homologues. D54 is a second-sphere residue in the active site that makes two

dx.doi.org/10.1021/bi2005398 | *Biochemistry* 2011, 50, 8603–8615

Table 2. Summary of Data Collection and Refinement Statistics for Native PhnP[a]

space group	*C*2
unit cell parameters	a = 110.7 Å, b = 75.3 Å, c = 82.4 Å, β = 125.5°
wavelength (Å)	1.033
resolution range (Å)	35.3−1.48 (1.497−1.480)
no. of observed reflections	1628375
no. of unique reflections	109380
completeness (%)	95.5 (76.0)
redundancy	7.1 (4.8)
R_{sym} (%)[b]	6.2 (43.1)
$\langle I/\sigma I\rangle$	48.3 (3.5)
R_{work} (%)[c]	16.1 (21.0)
R_{free} (%)	18.3 (23.0)
total no. of observations	87551
no. of observations for R_{free}	4388
root-mean-square deviation	
bond lengths (Å)	0.007
bond angles (deg)	1.235
mean temperature factor (Å^2)	15.5
no. of protein residues	497
no. of protein atoms	4048
no. of water atoms	521
no. of metal ions	6 (4 Mn, 2 Zn)
no. of orthovanadate ions	2
Ramachandran statistics (%)	
most favored regions	87.2
allowed regions	11.1
generously allowed regions	1
disallowed regions	0.7

[a]The values in parentheses are data for the high-resolution shell (1.497−1.480 Å). [b]$R_{sym} = \sum|I(k) - \langle I\rangle|/\sum I(k)$, where $I(k)$ and $\langle I\rangle$ represent the diffraction intensity values of the individual measurements and the corresponding mean values, respectively. The summation is over all measurements. [c]$R_{work} = \sum||F_o| - |F_c||/\sum|F_o|$, and $R_{free} = \sum||F_{o(free)}| - |F_{c(free)}||/\sum|F_{o(free)}|$, where F_o is the observed structure factor and F_c is the calculated structure factor based on the model. No σ cutoff was applied to the data; 5% of reflections were excluded from the refinement for the calculation of R_{free}.

ligand interactions, one with NE2 of metal ion ligand H81 (2.71 Å) and the second with the hydroxyl of T75 (2.8 Å), another second-sphere residue that stabilizes metal ion ligand H76 (Figure 1c). The dihedral angles for this residue are 66° (ϕ) and 170° (ψ) in both monomers. D54 is conserved among PhnP homologues[25,26] and, as described below, was targeted for substitution with alanine to probe its role in catalysis.

As observed previously, PhnP contains two distinct metal binding sites.[26] Each PhnP monomer contains a single zinc ion located ~17 Å from the active site (Figure 1a). The zinc ion is bound in a tetrahedral geometry by C19, C21, C23, and H225, forming a structure-stabilizing element. These coordinating residues are also uniquely conserved in the PhnP family. PhnP is copurified with substoichiometric amounts of manganese ion yet exhibits high specific activity with this metal ion.[26] Therefore, PhnP crystals were grown in the presence of 0.5 mM $MnCl_2$. This concentration is above the apparent K_M value for the metal ion [K_M^{app} = 130 μM (data not shown)] and was anticipated to favor a fully metal ion-loaded active site. Indeed, this appeared to be the case as each monomer active site contained two metal ions, which were accordingly assigned as manganese (Figure 1b). Both manganese and zinc ions produce some anomalous signal at the wavelength used for data collection [1.033 Å (Table 2)], as seen on an anomalous signal map, with a slightly stronger signal observed for the structural zinc ion. Further evidence of active site bound manganese ions was inferred from ICP-MS analysis of metal ion content (see below). The more solvent-exposed manganese ion, designated MnA, was calculated to have a full occupancy of 1, while the less solvent exposed ion, MnB, has an occupancy of 0.75 in one monomer and 0.8 in the other. The reduced occupancy of the MnB in the crystal structure may reflect weaker coordination of this ion compared to that of MnA.

Clear density is observed for orthovanadate in both active sites of dimeric PhnP where the inhibitor is bound in a tetrahedral configuration (Figure 1b). Essentially identical interactions are observed in each PhnP monomer. Two of the orthovanadate oxygens are engaged as metal ion ligands (O−Mn distances of 2.0 Å) to form an overall bridging complex between the two manganese ions (Figure 1c). A water molecule (or hydroxide) is likewise observed bridging the metal ions and further interacts with the carboxyl oxygen of D80, most likely through a hydrogen bond (O−O distance of 2.7 Å). D80 simultaneously acts as a ligand for MnB (O−Mn distance of 2.4 Å). The bridging water molecule thus appears to be ideally positioned for nucleophilic attack on the vanadate nucleus, which is only 2.9 Å away. The analogous configuration was previously observed with PhnP bound to (*S*)-malate (a crystallization additive) where the 2-hydroxyl of (*S*)-malate assumed the role of the bridging water molecule.[26] The third orthovanadate oxygen is oriented opposite to the "nucleophilic" water molecule above (O3−V−H_2O angle of 175°) and also forms a hydrogen bond with the putative general acid H200 (O−N distance of 2.6 Å). In this arrangement, it is tempting to speculate that the third oxygen resembles the "leaving group" of a phosphate diester prior to in-line attack by the bridging water molecule. Finally, the fourth orthovanadate oxygen faces the open space of the active site. The third and fourth orthovanadate oxygens are further solvated by water molecules.

A comparison of the PhnP−orthovanadate complex with the 1.27 Å structure of a phosphodiesterase from *B. melitensis* bound to guanosine 5′-monophosphate (PDB entry 3md7) reveals an essentially identical configuration for the 5′-phosphate (Figure 1d). Guanosine 5′-monophosphate is likely a product of the hydrolysis of guanosine 3′,5′-cyclic monophosphate. However, the function of this enzyme is unknown, and its gene does not appear to be associated with *phn* genes. Nevertheless, the degree of sequence and structural homology of this enzyme with PhnP is the highest among structurally characterized phosphodiesterases of the metallo-β-lactamase family (25% identical sequence; *Z* score = 27.6; root-mean-square deviation of 2.5 Å). Essentially identical interactions with inorganic phosphate are also described for *Bacillus subtilis* tRNase Z, but the lower resolution of this structure (2.1 Å) precluded an exact description of the interactions with the phosphate oxygens.[32]

Kinetic Analysis of PhnP Active Site Variants. Table 3 lists kinetic parameters for WT PhnP and variants containing single-amino acid substitutions within the active site. The metallo-β-lactamase superfamily contains four highly conserved sequence motifs that contribute residues for metal ion

Table 3. Kinetic parameters for the hydrolysis of bpNPP by PhnP mutant variants (pH 7.1, 25°C). Altered residues are highlighted in the active site scheme shown below

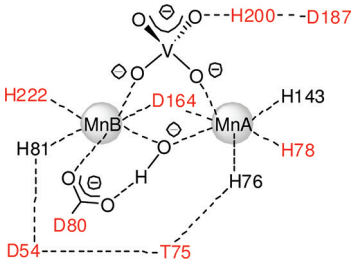

PhnP	k_{cat} (min^{-1})[a]	K_M (mM)[a]	k_{cat}/K_M (min^{-1} mM^{-1})	$(k_{cat}/K_M)^{mut}/(k_{cat}/K_M)^{WT}$
WT[b]	64 ± 2	3.5 ± 0.3	18	1
H200A	33 ± 4	18 ± 3	1.8	0.1
D187A	53 ± 4	3.4 ± 0.6	15	0.83
D80A[b]	0.050 ± 0.002	3.7 ± 0.4	0.013	7.2×10^{-4}
D164A	0.047 ± 0.003	3.7 ± 0.5	0.013	7.2×10^{-4}
H78A	0.20 ± 0.02	3.8 ± 0.8	0.053	2.9×10^{-3}
H222A	7.9 ± 0.4	3.0 ± 0.6	2.6	0.14
D54A	0.042 ± 0.002	2.4 ± 0.3	0.017	9.4×10^{-4}
T75A	15 ± 4	28 ± 10	0.54	0.030

[a]Kinetic parameters determined with 1 mM $MnCl_2$. [b]Kinetic parameters from ref 26.

coordination and catalysis.[30,45] Metal ion binding residues from motif II (H78 and D80 of the HxHxDH motif), motif IV (D164), and motif V (H222) were selected for mutagenesis to evaluate their contributions to catalysis of bpNPP hydrolysis. Large decreases of 345−1400-fold in k_{cat}/K_M are observed for D80A, D164A, and H78A PhnP, but only a 7-fold decrease is observed for H222A PhnP. All of the observed effects arose from reductions in k_{cat}, as K_M was unaffected. T75A PhnP and D54A PhnP were generated because, as noted by others,[25,32,46] these residues serve as "second-sphere" residues by forming a cyclic hydrogen bond network with the metal ion ligands H76 and H81 from motif II. Alteration of these neighboring residues had surprisingly different results: D54A PhnP showed a dramatic decrease in k_{cat}/K_M (1060-fold) and no significant change in K_M, whereas T75A PhnP showed a modest decrease in k_{cat}/K_M (33-fold), largely the result of an increase in K_M from 3.5 mM to approximately 30 mM. The large effect of the substitution of D54 is particularly notable because of the nontypical dihedral angles exhibited by this residue in the structure (see above). Residue H200 in PhnP is proposed to act as a general acid in homologous enzymes[31,32] and appears to be ideally positioned to play this role in the PhnP vanadate complex described above. Surprisingly, however, H200A PhnP displayed a 2-fold reduction in k_{cat}, while K_M increased nearly 6-fold (from 3.5 to 18 mM), yielding a modest 10-fold overall reduction in k_{cat}/K_M. The D187A variant echoes this modest effect. This second-sphere residue interacts with H200 through a 2.6 Å hydrogen bond and presumably modulates its ionization state. However, D187A PhnP has essentially WT kinetic parameters. The CD spectra of all PhnP mutant variants are essentially identical (Figure 2), indicating that alteration of the active site residues did not significantly impact the structural integrity of the fold. Therefore, the altered kinetic parameters observed here arise from local changes in the active site, specifically loss of the side chain and metal ion binding (see below), rather than a global change in enzyme structure.

ICP-MS Analysis. As reported previously, and reiterated in Table 4, WT PhnP is copurified with substoichiometric quantities of manganese ion (0.13 ± 0.05 per monomer) and

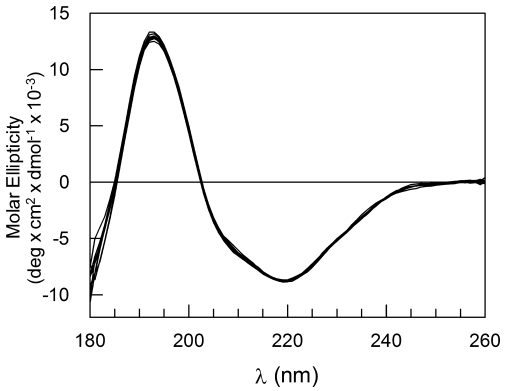

Figure 2. CD spectrum of WT PhnP superimposed with spectra of active site mutant variants listed in Table 3 (pH 7 and 20 °C).

approximately stoichiometric amounts of zinc ion (1.4 ± 0.1 per monomer) when isolated from *E. coli* grown in standard LB.[26] In contrast, D80A and D54A PhnP variants were purified free of manganese ions but retained stoichiometric amounts of zinc ion. This is consistent with weakly bound, active site manganese ions that are readily lost upon substitution of metal ion ligands (D80A) and second-sphere (D54A) residues. In contrast, the tightly bound structural zinc ion located ~17 Å from the active site is largely insensitive to these substitutions (Table 4). Similarly, it was shown that while manganese ions are readily stripped from WT PhnP with EDTA, yielding inactive enzyme, the structural zinc ion resists removal.[26] As shown in Table 4, greater manganese ion content of WT PhnP could be achieved by producing the enzyme in manganese ion-enriched cultures (0.7 ± 0.1 manganese ion per monomer) or incubating the purified enzyme with excess manganese ion followed by extensive dialysis (0.4 ± 0.1 manganese ion per monomer). The correlation between metal ion content and in vivo availability has been noted previously with metallo-β-lactamases.[47] Once again, metal ion affinity appears to be adversely affected by alteration of active site residues: all mutant variants were isolated either metal ion free (T75A, H78A,

dx.doi.org/10.1021/bi2005398 | *Biochemistry* 2011, 50, 8603–8615

Table 4. ICP-MS Analysis of Manganese and Zinc Ion Content in Purified WT PhnP and Its Variants[a]

		[Mn2+]/[PhnP]		
	[Zn2+]/[PhnP] in LB	LB	Mn-enriched LB[b]	Mn incubation[c]
WT	1.4 ± 0.1[d]	0.13 ± 0.05[d]	0.7 ± 0.1	0.4 ± 0.1
H200A	1.1 ± 0.1	0	0	0
D187A			0.15 ± 0.05	
D80A	1.0 ± 0.1[d]	0[d]	0.6 ± 0.1	0.16 ± 0.05
D164A			0	
H78A			0	
H222A			0	
D54A	0.9 ± 0.1	0	0.20 ± 0.05	
T75A			0	

[a]Average of three measurements based on 10 μM monomeric PhnP. Zero indicates the sample was indistinguishable from buffer alone. Blank field means not determined. [b]Proteins isolated from *E. coli* cultures grown in LB with 0.5 mM $MnCl_2$. [c]Purified proteins were incubated with 1 mM $MnCl_2$ and then dialyzed. [d]Data from ref 26.

D164A, H200A, and H222A) or with reduced metal ion content (D54A, D80A, and D187A) relative to the WT enzyme despite exposure to excess manganese ion in vivo or in vitro. However, all of the metal ion content values are considerably less than the two manganese ions per monomer observed in the crystal structure that was obtained in the presence of excess manganese ion. This likewise suggests weak binding to one or both of the metal ion sites (i.e.: MnA and MnB in Figure 1c) in the active site and would explain the saturating dependence of PhnP activity on manganese ion concentration [apparent K_M = 130 μM (data not shown)]. In sum, the reduced manganese ion affinities of PhnP active site variants indicate that the changes in kinetic parameters given in Table 3 can be partly ascribed to partial metal ion occupancy of the active site in addition to loss of the side chain in catalysis.

pH Dependence of WT and H200A PhnP. The k_{cat}/K_M value of WT PhnP for bpNPP hydrolysis in the presence of manganese ion exhibits a bell-shaped dependence on pH. A fit of this data to an equation describing the ionization of two enzymic residues afforded pK_{a1} and pK_{a2} values of 6.6 ± 0.2 and 7.2 ± 0.2, respectively (Figure 3). The nickel ion-activated WT

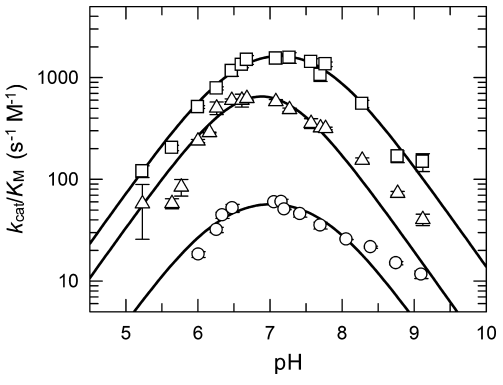

Figure 3. Variation of k_{cat}/K_M with pH for WT and H200A PhnP. Data shown for WT PhnP reacting with bpNPP in the presence of 1 mM $MnCl_2$ (△) or $NiCl_2$ (□) and H200A reacting with bpNPP and 1 mM $NiCl_2$ (○).

enzyme has a similar pH profile, with pK_{a1} and pK_{a2} values of 6.5 ± 0.1 and 7.8 ± 0.1, respectively. The pH dependence of H200A PhnP was also evaluated using nickel ion because this variant was not sufficiently active with manganese ion to accurately measure k_{cat}/K_M values at nonoptimal pH values. Like the WT enzyme, H200A PhnP exhibited a bell-shaped pH−rate profile defined by virtually identical ionizations: pK_{a1} = 6.3 ± 0.2, and pK_{a2} = 7.8 ± 0.2.

Brønsted Analysis of the PhnP Reaction. PhnP k_{cat}/K_M values were determined for a series of methyl phenylphosphate diesters with pK_a^{LG} values ranging from 4.09 to 9.99 (Table 5). A Brønsted plot of these values (Figure 4) revealed three classes of substrates based on reactivity. Each substrate class differs in the number of electron-withdrawing groups acting through resonance at the ortho or para positions. Such substituents allow stabilization of negative charge development on the leaving group phenolate oxygen. Substrates with no ortho or para electron-withdrawing groups (pK_a^{LG} = 7.85−9.99) afforded a Brønsted coefficient β_{lg} of −1.06 ± 0.06 with a correlation coefficient r of 0.997. In contrast, substrates with a single electron-withdrawing group at the ortho or para position (pK_a^{LG} = 5.04−7.95) yielded a lower Brønsted coefficient β_{lg}^{obs} of −0.65 ± 0.08 (r = 0.984). Finally, 2,4-dinitrophenyl methylphosphate (pK_a^{LG} = 4.09) is a single outlier because of the presence of two electron-withdrawing groups at the ortho and para positions. The difference in reactivity between the classes of substrates does not appear to be the result of a rate-limiting substrate binding or conformational change in PhnP as the viscosity dependence of k_{cat}/K_M for substrates from each group is weak and virtually identical (see the Supporting Information).

The Leffler α value, which provides the fractional effective charge on the phenolate oxygen in the transition state,[34] can be calculated from the ratio of β_{lg}/β_{eq}, where β_{eq} is the equilibrium Brønsted coefficient for the overall reaction (Scheme 1).[35,48,49] For the uncatalyzed hydrolysis of methyl phenylphosphate by hydroxide, the β_{eq} value is −1.74,[34,50] which leads to an α value of 0.61 (−1.06/−1.74) for the PhnP reaction. This indicates that the bond between the phenolate oxygen and phosphorus is 61% cleaved, which is consistent with a synchronous transition state for the transfer of phosphoryl to hydroxide that is intermediate between a fully associative or phosphorane transition state (β_{lg}/β_{eq} = 0) and a fully dissociative or metaphosphate transition state (β_{lg}/β_{eq} = 1).[35,48] The effective charge on the leaving group oxygen in the transition state can also be calculated.[50,51] On the basis of a β_{eq} of −1.74, the effective charge on the leaving group oxygen of the substrate in the ground state is 0.74 (this value is positive because phosphorus is more electronegative than hydrogen) and that of the phenolate product is −1 (the neutral phenol has a charge of 0). Therefore, the effective charge on the leaving group oxygen in the transition state is −0.32 (0.74 + β_{lg}^{obs} = 0.74 −

dx.doi.org/10.1021/bi2005398 | *Biochemistry* 2011, 50, 8603−8615

Table 5. PhnP k_{cat}/K_M Values for Hydrolysis of Substituted Methyl Phenylphosphate Diesters (pH 7.1 and 25°C)

substituent	pK_a^{LG}	WT k_{cat}/K_M (s^{-1} M^{-1})	H200A k_{cat}/K_M (s^{-1} M^{-1})	$(k_{cat}/K_M)^{H200A}/(k_{cat}/K_M)^{WT}$
2,4-$(NO_2)_2$	4.09	220 ± 10	38 ± 1	0.17
2,5-$(NO_2)_2$	5.04	680 ± 60		
2-Cl-4-NO_2	5.45	290 ± 30		
4-NO_2	7.14	47 ± 4	5.3 ± 0.3	0.11
2,4-$(Cl)_2$	7.85	124 ± 5		
4-CN	7.95	6.0 ± 0.3		
3-NO_2	8.39	41 ± 2	2.2 ± 0.2	0.054
4-Cl	9.38	2.4 ± 0.2		
H	9.99	0.90 ± 0.03		

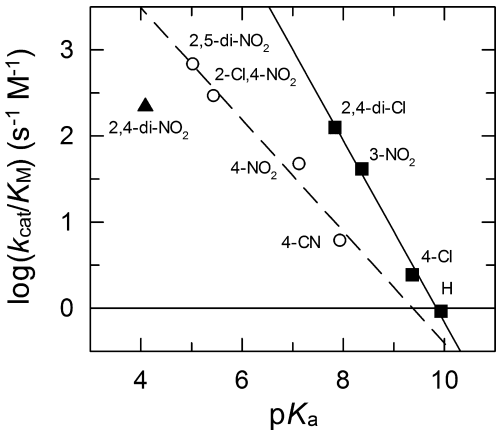

Figure 4. Brønsted plot of WT PhnP k_{cat}/K_M values for a series of methyl phenylphosphate diesters. Each point is labeled with the type of substitution of the substrate and according to the ability to act through resonance to stabilize a phenolate anion: (■) no resonance active substituents ortho or para to the phenolate oxygen, (○) a single resonance active substituent ortho or para to the phenolate oxygen, and (▲) two resonance active substituents ortho and para to the phenolate oxygen. A linear fit of the ■ data points (—) yields a β_{lg} of −1.06 ± 0.06, whereas a fit of the ○ data (– – –) gives a β_{lg} of −0.65 ± 0.08.

1.06 = −0.32). This partial negative charge is also consistent with a synchronous transition state in which the phosphorus oxygen bond still has considerable bond order or, alternatively, a greater degree of bond cleavage with compensating charge neutralization from an active site residue or metal ion.

■ DISCUSSION

PhnP−Orthovanadate Complex. Orthovanadate is a close structural mimic of inorganic phosphate. The vanadate nucleus can also accept a fifth oxygen ligand to adopt a structure that resembles the trigonal bipyramidal phosphorane transition state for an associative mechanism of phosphodiester hydrolysis (reviewed in ref 52). Cyclic nucleotides bearing pentavalent vanadate have been generated in situ in the active sites of ribonuclease A[53] and *Arabidopsis thaliana* cyclic nucleotide phosphodiesterase during crystallization.[54] Because PhnP regiospecifically hydrolyzes 5-phospho-α-D-ribosyl 1,2-cyclic phosphate in vivo,[26] we followed these examples to generate the corresponding cyclic vanadate ester in situ by adding a mixture of orthovanadate and 5-phospho-D-ribose to PhnP crystals. Unfortunately, we were unable to generate crystals of this complex with sufficient quality for X-ray analysis. Nevertheless, high-quality crystals were obtained with only orthovanadate as the additive (final concentration of 0.5 mM). Orthovanadate displays mixed inhibition with PhnP [K_I = 13 ± 3 μM; K_I' = 44 ± 17 μM (see the Supporting Information)], which may be attributed to the dimeric structure and the cooperative behavior common to this enzyme[26] and other tRNases of the metallo-β-lactamase family.[32,55,56] Phosphate, in contrast, is a weaker inhibitor (K_I = 230 ± 30 μM). The high resolution of this structure clearly shows orthovanadate bound in a "ground-state" tetrahedral configuration, rather than the "phosphorane" transition-state configuration for which we had hoped. Nevertheless, an appropriate configuration for phosphoryl transfer is observed with this phosphate mimic. The structure clearly supports a dual role for D80 as a ligand for one of the active site metal ions while simultaneously positioning the metal ion-bound nucleophilic water molecule or hydroxide. In the case of bound water, D80 may also act as a general base, although the interaction with the Lewis acidic metal ion can be expected to reduce basicity. H200 is positioned to donate a proton to a leaving group that is opposite of the incoming water nucleophile. The vanadate complex also clearly shows how both metal ions could participate in stabilizing the accumulation of negative charge on the nonbridging oxygens of a phosphate diester as the nucleophile attacks. The excellent alignment of bound ligands, metal ions, nucleophilic waters, and active site residues of PhnP and the *B. melitensis* phosphodiesterase suggests that the mechanism for hydrolysis of cyclic phosphate diesters is likely conserved between these two enzymes. A model of the PhnP in vivo substrate bound to the active site was created using the orthovanadate as a guide (Figure 5). The model suggests that H200 could productively interact with the leaving group 2-hydroxyl of the ribose, leading to the α-D-ribosyl 1,5-bisphosphate product observed in vivo, while R89 and H113 of the other monomer could electrostatically stabilize the 5-phosphate of the substrate.

Contributions of Active Site Residues to Catalysis. H200 has been proposed to act as a general acid catalyst during phosphodiester hydrolysis in related enzymes.[30,31] The complex of PhnP with orthovanadate indeed supports this assignment, with H200 interacting with the leaving group oxygen of the inhibitor. However, kinetic analysis of H200A PhnP reveals a diminished role for this residue in proton donation (Tables 3 and 5) as only a modest reduction is observed in k_{cat}/K_M (6−19-fold) with bpNPP and methyl phenylphosphate diesters with widely differing leaving groups (pK_a^{LG} = 4.09−8.39). This modest reduction may in part be due to the relatively poor efficiency of these artificial substrates. Nevertheless, this result clearly differs from those for related phosphodiesterases, which experience 500−11000-fold decreases in k_{cat}/K_M with RNA or bpNPP substrates when the equivalent residue is deleted.[30,31,57] H200A PhnP also has a pH−rate profile with pK_{a1} and pK_{a2} values that are within error of those of the WT enzyme. In a

Scheme 1. Brønsted Analysis and Proposed Mechanism for the PhnP Reaction

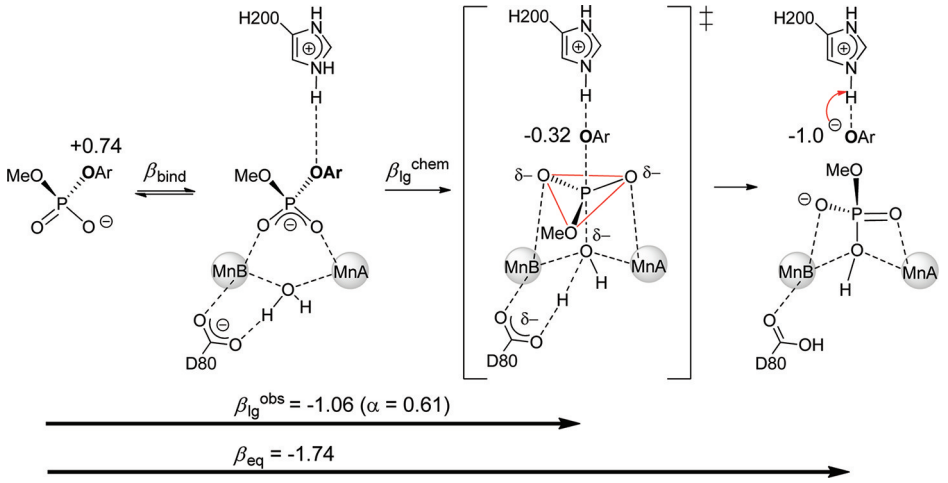

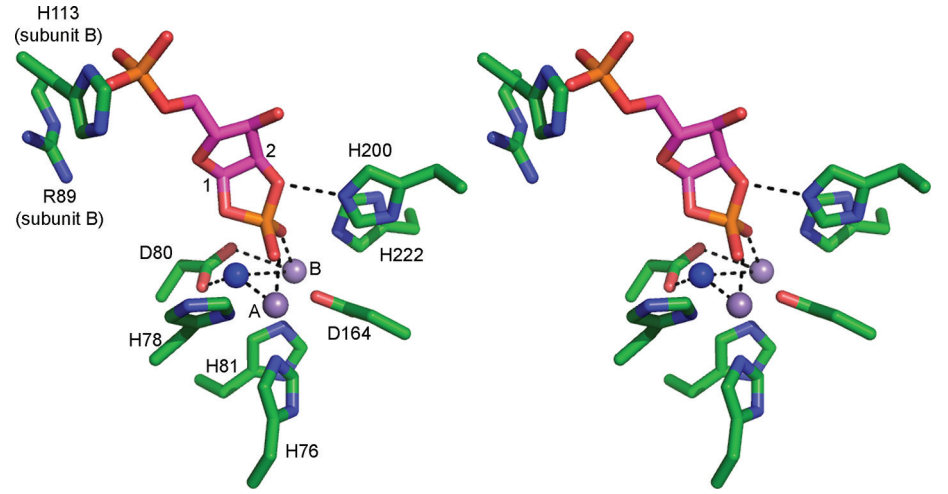

Figure 5. Wall-eyed stereoview of a model of the in vivo PhnP substrate 5-phospho-α-D-ribosyl 1,2-cyclic phosphate (pink) bound to the active site. The cyclic phosphate was superimposed with the bound orthovanadate (not shown). Ribose carbons 1 and 2 are indicated.

simple ionization scenario, the more basic limb (pK_{a2} = 7.8) should shift or disappear entirely upon deletion of a general acid catalyst. All of this suggests that H200 is not involved in the significant transfer of protons to the leaving group in the transition state, at least with activated substrates. This may be an evolutionary outcome of the inherent strain in the 1,2-cyclic phosphate of the natural substrate that would reduce the need for protonic assistance. Such strain is starkly exhibited in the 10^6-fold greater rate of hydrolysis of ethylene phosphate compared to that of dimethyl phosphate.[58] The equivalent residue in *E. coli* tRNase ZipD, H248, has been suggested to trigger cooperativity in the dimeric enzyme upon interacting with the bound substrate.[55] A similar role can be envisioned for H200 in PhnP, which also exhibits weak cooperativity.[26]

D80A PhnP displayed one of the largest decreases in k_{cat}/K_M. Using the PhnP−orthovanadate complex as a guide, the large decrease in this parameter is consistent with a dual role in metal ion binding (MnB) and positioning the metal ion-bound water or hydroxide for nucleophilic attack on the phosphorus center. Large effects are also observed for the tRNases upon alteration of this residue,[30,31,46,57] and a mechanistically similar role has been proposed for the metallo-β-lactamase reaction.[59−65] Likewise, by analogy to the metallo-β-lactamases, the more acidic pK_{a1} of the pH−rate profile (Figure 3) may correspond to ionization of the metal ion-bound water.[66,67]

Alteration of other active site residues revealed differential effects on catalysis, despite seemingly similar structural roles for these residues. The large decrease in k_{cat}/K_M for the D164A variant is consistent with its role as a bridging ligand for both active site metal ions. However, alteration of H78 and H222, ligands for MnA and MnB, respectively, revealed that H78 is essential for catalysis whereas H222 is almost dispensable. Alteration of second-sphere residues D54 and T75 in PhnP also revealed surprisingly different effects on k_{cat} and K_M parameters despite their similar roles in stabilizing metal ion ligands H81 and H76. In contrast, alteration of any of these residues in related tRNases universally causes large decreases in k_{cat}/K_M.[30,31,46,57]

Active Site Metal Ions. Despite having a clear preference for manganese and nickel ions for catalysis, WT PhnP has relatively weak affinity for these ions.[26] The enzyme cannot be isolated in a fully loaded state of two metal ions per active site, even after incubation or synthesis in the presence of excess metal. The relatively weak affinity of the PhnP active site for manganese ion contrasts with the higher affinity for zinc ion displayed by *E. coli* tRNase ZipD (K_d = 2−26 μM) and *A. thaliana* tRNase Z,[68,69] both of which can be isolated with two

dx.doi.org/10.1021/bi2005398 | *Biochemistry* 2011, 50, 8603−8615

metal ions per active site (the latter case can even resist treatment with chelating agents). This is notable because these enzymes share identical active site residues[26] and suggests that more subtle effects, achieved through sequence differences remote from the active site, tune the active site preference and affinity for metal ions and substrates (as elegantly illustrated by directed evolution studies with metallo-β-lactamases[70]). The weak affinity of PhnP for active site metal ions also raises the question of how catalysis might be achieved in vivo where low metal ion concentrations may be expected. For similar reasons, catalysis with a single, tightly bound metal ion has been proposed to occur with metallo-β-lactamases in vivo[71,72] and cannot be excluded for phosphodiester hydrolysis by tRNases when metal ion concentrations are low,[28,68] although some controversy about the viability of the mononuclear state remains.[73] When synthesized in *E. coli* grown in manganese ion-enriched medium, PhnP can be isolated with approximately one manganese ion per monomer (Table 4). However, it is not clear that this represents a metal ion bound to one position of the active site or distributed over both positions (i.e., MnA and MnB). The latter scenario is quite plausible, as PhnP containing ~0.13 manganese ion per monomer was crystallized with a dinuclear active site (suggesting selective crystallization of the dinuclear enzyme).[26,41] In any case, PhnP is clearly catalytically competent and achieves its greatest activity in the presence of excess manganese ion where a dinuclear active site is expected, and indeed observed in the crystal structure generated in the presence of excess manganese ion. Interestingly, *E. coli* possesses a manganese ion sensory protein, MntR, that regulates the expression of *mntH*, encoding a transporter for manganese ion uptake[74] that can increase cytoplasmic manganese ion concentrations to >300 μM (and under certain conditions to 1−3 mM).[75] Although these high concentrations do not entirely represent free manganese ion, these values are in excess of the apparent K_M for the metal ion displayed by PhnP and could yield maximal activity. In *E. coli* and several other species of bacteria, it is commonly observed that the cytoplasmic manganese ion concentration is typically highest when the cells are slow-growing or in stasis,[75] as would be expected when they are deprived of nutrients such as inorganic phosphate. This is precisely the scenario under which the *phnP* gene would be expressed. Thus, a simultaneous increase in cytoplasmic manganese ion concentration would stimulate PhnP activity when it is most needed, as has been proposed for a large number of other bacterial enzymes (reviewed in ref 75). Interestingly, some tRNases of the metallo-β-lactamase family also show enhanced bpNPP activity in the presence of manganese ion and even require this metal ion for hydrolysis of tRNA.[69,76]

It is evident that part of the effect of each active site substitution in PhnP is to reduce the fraction of fully metal ion-loaded and catalytically competent enzyme. All active site mutant variants, with the exception of D80A PhnP, were obtained in metal ion-depleted or apo form when produced from manganese ion-enriched cultures. This is even the case for substitutions that affect residues that do not directly act as metal ion ligands (i.e., D54A, T75A, and H200A), indicating that metal ion affinity is highly sensitive to the local environment. Interestingly, the activity of some tRNase mutant variants toward tRNA has been "rescued" upon addition of manganese ion, suggesting a more complex role for this metal ion, such as mixed manganese ion/zinc ion loading of the active sites, or a role for manganese ion in forming a sensitive conformation of the tRNA substrate.[31,69] Mixed metal ion active sites are a feature of some members of the metallo-β-lactamase family, with glyoxalase II being a prominent example.[77] Surprisingly, glyoxalase II utilizes the same active site residues as *E. coli* tRNase ZipD and PhnP for metal ion coordination,[57] highlighting once again the subtle role of structure and residues remote from the active site in tuning metal ion preferences. A mixed metal ion active site for PhnP may also be a possibility in vivo, although the enzyme is 40−73-fold less active when zinc ion is included with the preferred metal ions, manganese and nickel.[26]

Brønsted Analysis of the PhnP Transition State. Analysis of the leaving group dependence of the PhnP reaction in a Brønsted plot revealed two linear relationships that can be attributed to resonance effects. The β_{lg}^{obs} value of −1.06 ± 0.06 for the reaction of PhnP with methyl phenylphosphates lacking ortho and para resonance active substituents is essentially identical to that observed for the nonenzymatic reaction with hydroxide ion (−0.94 ± 0.05),[35] implying very similar transition-state structures for both reactions. The lower β_{lg} value of −0.65 ± 0.08 for substrates containing ortho or para resonance active substituents appears to suggest a "tighter" transition state in which the nucleophile and leaving group oxygens are more closely associated with the phosphorus center. However, it is more likely the reduced β_{lg} value is due to resonance-induced binding effects, which have been observed previously with alkaline phosphatase.[35,42,78] Because k_{cat}/K_M represents substrate binding to the free enzyme as well as the rate-limiting chemical step on the enzyme (or first irreversible step), the observed β_{lg} value is likewise a composite of Brønsted coefficients for substrate binding and the rate-limiting chemical step (eq 3):

$$\beta_{lg}^{obs} = \beta_{bind} + \beta_{lg}^{chem} \quad (3)$$

If reactivity depended on only the pK_a of the leaving group, then β_{lg}^{chem} alone would be sufficient to rationalize β_{lg}^{obs}. However, substituents at the ortho and para positions can resonance stabilize negative charge development on the phenolate and nonbridging phosphate oxygens. This will significantly weaken binding of these oxygens to active site residues and metal ions, thereby reducing β_{bind} and β_{lg}^{obs}. The PhnP−orthovanadate complex reveals that both metal ions could participate in binding nonbridging oxygens, leading to this resonance effect.

Because the β_{lg}^{obs} value of −1.06 ± 0.06 is presumably free of resonance effects, this value is likely representative of the biologically relevant reaction. Calculation of the corresponding Leffler α value suggests that, at a minimum, the bond to the phenolate oxygen is 61% cleaved and the leaving group oxygen bears a fractional effective charge of −0.32. This can be interpreted as representing synchronous bond formation and cleavage with the nucleophile and leaving group in the transition state (i.e., intermediate between fully associative and dissociative mechanisms). Alternatively, these values can also conform to a completely broken phosphorus−leaving group bond (i.e., fully dissociative transition state) with simultaneous partial neutralization of the leaving group oxygen by an active site metal ion or general acid residue.

Scheme 1 summarizes the structural and kinetic data for PhnP, along with the Brønsted parameters for the reaction. The scheme is based on the orthovanadate complex that appears to represent an ideal configuration for in-line attack of the

nucleophilic (or hydroxide) on a phosphate diester. In this mechanism, the two manganese ions reduce the pK_a of the attacking water molecule, the nucleophilicity of which may be further enhanced by deprotonation by D80. H200 is assumed to be protonated because of its proximity to a negatively charged substrate and its interaction with D187. However, H200 does not contribute substantially to transition-state stabilization as a general acid but instead delivers a proton to the leaving group after the rate-determining step. This would be consistent with the minor contribution of this residue to k_{cat}/K_M with aryl phosphate diesters.

■ CONCLUSIONS

By combining structural, kinetic, and linear free energy relationship analyses, we were able to examine the PhnP phosphodiesterase reaction in fine detail. The high-resolution structure of the phosphate analogue orthovanadate bound to the dinuclear active site of PhnP reveals an ideal arrangement phosphoryl transfer involving in-line attack of a metal ion-bound hydroxide, stabilization of phosphate nonbridging oxygens by the metal ions, and the potential for H200 to stabilize the leaving group oxygen as a general acid catalyst. Substantial negative charge detected on the leaving group oxygen by Brønsted analysis likewise suggests that general acid stabilization would be beneficial. However, site-directed mutagenesis and reaction with a variety of substrates reveal a minor role for H200 in the transition state, unlike the large contributions observed for the equivalent residue in tRNase Z phosphodiesterases. This suggests that leaving group stabilization is not a major component of the activation barrier for the PhnP reaction, which may be an evolutionary outcome of the strain present in the cyclic phosphate diester of the natural substrate. PhnP also exhibits substantial differences with respect to related phosphodiesterases with minor contributions of H222 (metal ion binding) and T75 (second-sphere residue) to catalysis. Overall, the differences between PhnP and other phosphodiesterases may reflect evolutionary plasticity in these enzymes, where catalytic residues, through divergent evolution, assume different roles (or relative contributions) as their respective reactions become more specialized.

■ ASSOCIATED CONTENT

Supporting Information

Synthetic procedures for the preparation of substituted methyl phenylphosphates, NMR spectroscopic data (^{1}H and ^{31}P), analysis of inhibition of PhnP by orthovanadate and phosphate, and dependence of PhnP reaction rates on viscosity. This material is available free of charge via the Internet at http://pubs.acs.org.

Accession Codes

The atomic coordinates for the PhnP−orthovanadate complex have been deposited in the Protein Data Bank as entry 3P2U.

■ AUTHOR INFORMATION

Corresponding Author

*Department of Chemistry, Chernoff Hall, Queen's University, Kingston, ON K7L 3N6, Canada. Phone: (613) 533-3259. Fax: (613) 533-6669. E-mail: dlzechel@chem.queensu.ca.

Funding

This work was supported by the Natural Sciences and Engineering Research Council of Canada (NSERC), the Canadian Institutes of Health Research, and the Canadian Foundation for Innovation. M. Wathier was supported by a NSERC undergraduate summer research award. B.H.-J. thanks the Danish Council for Independent Research, Natural Sciences, for funding. D.L.Z. is additionally supported by an Early Researcher Award, and Z.J. is a Canada Research Chair in Structural Biology.

■ ACKNOWLEDGMENTS

We thank our colleagues in the Department of Chemistry, Professor R. Stan Brown and Tony Liu, for insightful discussions concerning linear free energy relationships and generous gifts of substituted methyl phenylphosphates, and Professor Dianne Beauchemin for assistance with ICP-MS analyses. We also thank Yoonmi Margaret Kim and Frederic Faucher of the Department of Biochemistry, Queen's University, for assistance in protein purification, crystallization, and structure refinement. Finally, we thank Kim Munro of the Protein Function Discovery unit, Queen's University, for performing the CD spectrometric analyses.

■ ABBREVIATIONS

PhnP, phosphodiesterase encoded by *phnP* in the *E. coli phn* operon; bpNPP, bis(*p*-nitrophenyl)phosphate; WT, wild type; BSA, bovine serum albumin; PCR, polymerase chain reaction; ICP-MS, inductively coupled plasma mass spectrometry; HEPES, 4-(2-hydroxyethyl)-1-piperazineethanesulfonic acid; MES, 2-(*N*-morpholino)ethanesulfonic acid; BES, *N*,*N*-bis(2-hydroxyethyl)-2-aminoethanesulfonic acid; LB, lysogeny broth; pK_a^{LG}, pK_a of the conjugate acid of a leaving group.

■ REFERENCES

(1) Wackett, L. P., Wanner, B. L., Venditti, C. P., and Walsh, C. T. (1987) Involvement of the phosphate regulon and the *psiD* locus in carbon-phosphorus lyase activity of *Escherichia coli* K-12. *J. Bacteriol. 169*, 1753−1756.

(2) Chen, C. M., Ye, Q. Z., Zhu, Z. M., Wanner, B. L., and Walsh, C. T. (1990) Molecular biology of carbon-phosphorus bond cleavage. Cloning and sequencing of the *phn* (*psiD*) genes involved in alkylphosphonate uptake and C-P lyase activity in *Escherichia coli* B. *J. Biol. Chem. 265*, 4461−4471.

(3) Metcalf, W. W., and Wanner, B. L. (1991) Involvement of the *Escherichia coli phn* (*psiD*) gene cluster in assimilation of phosphorus in the form of phosphonates, phosphite, P_i esters, and P_i. *J. Bacteriol. 173*, 587−600.

(4) Cordeiro, M., Pompliano, D., and Frost, J. (1986) Degradation and detoxification of organophosphonates: Cleavage of the carbon to phosphorus bond. *J. Am. Chem. Soc. 108*, 332−334.

(5) Zeleznick, L. D., Myers, T. C., and Titchener, E. B. (1963) Growth of *Escherichia coli* on methyl- and ethylphosphonic acids. *Biochim. Biophys. Acta 78*, 546−547.

(6) Wackett, L. P., Shames, S. L., Venditti, C. P., and Walsh, C. T. (1987) Bacterial carbon-phosphorus lyase: Products, rates, and regulation of phosphonic and phosphinic acid metabolism. *J. Bacteriol. 169*, 710−717.

(7) Vera, M., Pagliai, F., Guiliani, N., and Jerez, C. A. (2008) The chemolithoautotroph *Acidithiobacillus ferrooxidans* can survive under phosphate-limiting conditions by expressing a C-P lyase operon that allows it to grow on phosphonates. *Appl. Environ. Microbiol. 74*, 1829−1835.

(8) Dyhrman, S. T., Chappell, P. D., Haley, S. T., Moffett, J. W., Orchard, E. D., Waterbury, J. B., and Webb, E. A. (2006) Phosphonate utilization by the globally important marine diazotroph *Trichodesmium*. *Nature 439*, 68−71.

(9) Huang, J., Su, Z., and Xu, Y. (2005) The evolution of microbial phosphonate degradative pathways. *J. Mol. Evol. 61*, 682−690.

(10) Iqbal, S., Parker, G., Davidson, H., Moslehi-Rahmani, E., and Robson, R. L. (2004) Reversible phase variation in the *phnE* gene, which is required for phosphonate metabolism in *Escherichia coli* K-12. *J. Bacteriol. 186*, 6118−6123.
(11) Metcalf, W. W., and Wanner, B. L. (1993) Mutational analysis of an *Escherichia coli* fourteen-gene operon for phosphonate degradation, using TnphoA′ elements. *J. Bacteriol. 175*, 3430−3442.
(12) Rizk, S. S., Cuneo, M. J., and Hellinga, H. W. (2006) Identification of cognate ligands for the *Escherichia coli phnD* protein product and engineering of a reagentless fluorescent biosensor for phosphonates. *Protein Sci. 15*, 1745−1751.
(13) Gebhard, S., and Cook, G. M. (2008) Differential regulation of high-affinity phosphate transport systems of *Mycobacterium smegmatis*: Identification of PhnF, a repressor of the *phnDCE* operon. *J. Bacteriol. 190*, 1335−1343.
(14) Frost, J., Loo, S., Cordeiro, M., and Li, D. (1987) Radical-based dephosphorylation and organophosphonate biodegradation. *J. Am. Chem. Soc. 109*, 2166−2171.
(15) Shames, S.L., Wackett, L. P., LaBarge, M., Kuczkowski, R., and Walsh, C. T. (1987) Fragmentation and stereochemical isomerization probes for homolytic carbon to phosphorus bond scission catalyzed by bacterial carbon-phosphorus lyase. *Bioorg. Chem. 15*, 366−373.
(16) Ahn, Y., Ye, Q., Cho, H., Walsh, C. T., and Floss, H. (1992) Stereochemistry of carbon-phosphorus cleavage in ethylphosphonate catalyzed by CP-lyase from *Escherichia coli*. *J. Am. Chem. Soc. 114*, 7953−7954.
(17) Adams, M. A., Luo, Y., Hove-Jensen, B., He, S. M., van Staalduinen, L. M., Zechel, D. L., and Jia, Z. (2008) Crystal structure of PhnH: An essential component of carbon-phosphorus lyase in *Escherichia coli*. *J. Bacteriol. 190*, 1072−1083.
(18) Yakovleva, G. M., Kim, S. K., and Wanner, B. L. (1998) Phosphate-independent expression of the carbon-phosphorus lyase activity of *Escherichia coli*. *Appl. Microbiol. Biotechnol. 49*, 573−578.
(19) Jochimsen, B., Lolle, S., McSorley, F. R., Nabi, M., Stougaard, J., Zechel, D. L., and Hove-Jensen, B. (2011) Five phosphonate operon gene products as components of a multi-subunit complex of the carbon-phosphorus lyase pathway. *Proc. Natl. Acad. Sci. U.S.A. 108*, 11393−11398.
(20) Errey, J. C., and Blanchard, J. S. (2006) Functional annotation and kinetic characterization of PhnO from *Salmonella enterica*. *Biochemistry 45*, 3033−3039.
(21) Avila, L., Loo, S., and Frost, J. (1987) Chemical and mutagenic analysis of aminomethylphosphonate biodegradation. *J. Am. Chem. Soc. 109*, 6758−6764.
(22) Hove-Jensen, B., Rosenkrantz, T. J., Haldimann, A., and Wanner, B. L. (2003) *Escherichia coli phnN*, encoding ribose 1,5-bisphosphokinase activity (phosphoribosyl diphosphate forming): Dual role in phosphonate degradation and NAD biosynthesis pathways. *J. Bacteriol. 185*, 2793−2801.
(23) Hove-Jensen, B., McSorley, F. R., and Zechel, D. L. (2011) Physiological role of *phnP*-specified phosphoribosyl cyclic phosphodiesterase in catabolism of organophosphonic acids by the carbon-phosphorus lyase pathway. *J. Am. Chem. Soc. 133*, 3617−3624.
(24) Aravind, L. (1999) An evolutionary classification of the metallo-β-lactamase fold proteins. *In Silico Biol. 1*, 69−91.
(25) Daiyasu, H., Osaka, K., Ishino, Y., and Toh, H. (2001) Expansion of the zinc metallo-hydrolase family of the β-lactamase fold. *FEBS Lett. 503*, 1−6.
(26) Podzelinska, K., He, S. M., Wathier, M., Yakunin, A., Proudfoot, M., Hove-Jensen, B., Zechel, D. L., and Jia, Z. (2009) Structure of PhnP, a phosphodiesterase of the carbon-phosphorus lyase pathway for phosphonate degradation. *J. Biol. Chem. 284*, 17216−17226.
(27) Hove-Jensen, B., Rosenkrantz, T. J., Zechel, D. L., and Willemoes, M. (2010) Accumulation of intermediates of the carbon-phosphorus lyase pathway for phosphonate degradation in *phn* mutants of *Escherichia coli*. *J. Bacteriol. 192*, 370−374.
(28) Spath, B., Canino, G., and Marchfelder, A. (2007) tRNase Z: The end is not in sight. *Cell. Mol. Life Sci. 64*, 2404−2412.
(29) Redko, Y., Sierra-Gallay, I., and Condon, C. (2007) When all's zed and done: The structure and function of RNase Z in prokaryotes. *Nat. Rev. Microbiol. 5*, 279−286.
(30) Karkashon, S., Hopkinson, A., and Levinger, L. (2007) tRNase Z catalysis and conserved residues on the carboxy side of the His cluster. *Biochemistry 46*, 9380−9387.
(31) Minagawa, A., Takaku, H., Ishii, R., Takagi, M., Yokoyama, S., and Nashimoto, M. (2006) Identification by Mn^{2+} rescue of two residues essential for the proton transfer of tRNase Z catalysis. *Nucleic Acids Res. 34*, 3811−3818.
(32) de la Sierra-Gallay, I. L., Pellegrini, O., and Condon, C. (2005) Structural basis for substrate binding, cleavage and allostery in the tRNA maturase RNase Z. *Nature 433*, 657−661.
(33) Crowder, M. W., Spencer, J., and Vila, A. J. (2006) Metallo-β-lactamases: Novel weaponry for antibiotic resistance in bacteria. *Acc. Chem. Res. 39*, 721−728.
(34) Ba-Saif, S. A., Davis, A. M., and Williams, A. (1989) Effective charge distribution for attack of the phenoxide ion on aryl methyl phosphate monoanion: Studies related to the action of ribonuclease. *J. Org. Chem. 54*, 5483−5486.
(35) Zalatan, J.G., and Herschlag, D. (2006) Alkaline phosphatase mono- and diesterase reactions: Comparative transition state analysis. *J. Am. Chem. Soc. 128*, 1293−1303.
(36) Otwinowski, Z., and Minor, W. (1997) Processing of X-ray diffraction data collected in oscillation mode. *Methods Enzymol. 276*, 307−326.
(37) Murshudov, G. N., Vagin, A. A., and Dodson, E. J. (1997) Refinement of macromolecular structures by the maximum-likelihood method. *Acta Crystallogr. D53*, 240−255.
(38) Adams, P. D., Grosse-Kunstleve, R. W., Hung, L. W., Ioerger, T. R., McCoy, A. J., Moriarty, N. W., Read, R. J., Sacchettini, J. C., Sauter, N. K., and Terwilliger, T. C. (2002) PHENIX: Building new software for automated crystallographic structure determination. *Acta Crystallogr. D58*, 1948−1954.
(39) Emsley, P., and Cowtan, K. (2004) Coot: Model-building tools for molecular graphics. *Acta Crystallogr. D60*, 2126−2132.
(40) Holm, L., and Park, J. (2000) DaliLite workbench for protein structure comparison. *Bioinformatics 16*, 566−567.
(41) Podzelinska, K., He, S., Soares, A., Zechel, D., Hove-Jensen, B., and Jia, Z. (2008) Expression, purification and preliminary diffraction studies of PhnP. *Acta Crystallogr. F64*, 554−557.
(42) Hollfelder, F., and Herschlag, D. (1995) The nature of the transition state for enzyme-catalyzed phosphoryl transfer. Hydrolysis of O-aryl phosphorothioates by alkaline phosphatase. *Biochemistry 34*, 12255−12264.
(43) Kempton, J. B., and Withers, S. G. (1992) Mechanism of *Agrobacterium* β-glucosidase: Kinetic studies. *Biochemistry 31*, 9961−9969.
(44) Leatherbarrow, R. J. (2007) *GraFit*, version 6, Erithacus Sofware Ltd., Horley, U.K.
(45) Ishii, R., Minagawa, A., Takaku, H., Takagi, M., Nashimoto, M., and Yokoyama, S. (2005) Crystal structure of the tRNA 3′ processing endoribonuclease tRNase Z from *Thermotoga maritima*. *J. Biol. Chem. 280*, 14138−14144.
(46) Zareen, N., Yan, H., Hopkinson, A., and Levinger, L. (2005) Residues in the conserved His domain of fruit fly tRNase Z that function in catalysis are not involved in substrate recognition or binding. *J. Mol. Biol. 350*, 189−199.
(47) Hu, Z., Gunasekera, T. S., Spadafora, L., Bennett, B., and Crowder, M. W. (2008) Metal content of metallo-β-lactamase L1 is determined by the bioavailability of metal ions. *Biochemistry 47*, 7947−7953.
(48) O'Brien, P. J., and Herschlag, D. (2002) Alkaline phosphatase revisited: Hydrolysis of alkyl phosphates. *Biochemistry 41*, 3207−3225.
(49) O'Brien, P. J., and Herschlag, D. (1999) Does the active site arginine change the nature of the transistion state for alkaline phosphatase catalyzed phosphoryl transfer? *J. Am. Chem. Soc. 121*, 11022−11023.

(50) Bourne, N., and Williams, A. (1984) Effective charge on oxygen in phosphoryl group transfer from and oxygen donor. *J. Org. Chem. 49*, 1200−1204.
(51) Deacon, T., Farrar, C. R., Sikkel, B. J., and Williams, A. (1978) Reactions of nucleophiles with strained cyclic sulfonate esters. Bronsted relationships for rate and equilibrium constants for variation of phenolate anion nucleophile and leaving group. *J. Am. Chem. Soc. 100*, 2525−2534.
(52) Davies, D. R., and Hol, W. G. (2004) The power of vanadate in crystallographic investigations of phosphoryl transfer enzymes. *FEBS Lett. 577*, 315−321.
(53) Ladner, J. E., Wladkowski, B. D., Svensson, L. A., Sjolin, L., and Gilliland, G. L. (1997) X-ray structure of a ribonuclease A-uridine vanadate complex at 1.3 Å resolution. *Acta Crystallogr. D53*, 290−301.
(54) Hofmann, A., Grella, M., Botos, I., Filipowicz, W., and Wlodawer, A. (2002) Crystal structures of the semireduced and inhibitor-bound forms of cyclic nucleotide phosphodiesterase from *Arabidopsis thaliana*. *J. Biol. Chem. 277*, 1419−1425.
(55) Kostelecky, B., Pohl, E., Vogel, A., Schilling, O., and Meyer-Klaucke, W. (2006) The crystal structure of the zinc phosphodiesterase from *Escherichia coli* provides insight into function and cooperativity of tRNase Z-family proteins. *J. Bacteriol. 188*, 1607−1614.
(56) de la Sierra-Gallay, I. L., Mathy, N., Pellegrini, O., and Condon, C. (2006) Structure of the ubiquitous 3′ processing enzyme RNase Z bound to transfer RNA. *Nat. Struct. Mol. Biol. 13*, 376−377.
(57) Vogel, A., Schilling, O., and Meyer-Klaucke, W. (2004) Identification of metal binding residues for the binuclear zinc phosphodiesterase reveals identical coordination as glyoxalase II. *Biochemistry 43*, 10379−10386.
(58) Thatcher, G., and Kluger, R. (1989) Mechanism and catalysis of nucleophilic substitution in phosphate esters. *Adv. Phys. Org. Chem. 25*, 99−265.
(59) Crisp, J., Conners, R., Garrity, J. D., Carenbauer, A. L., Crowder, M. W., and Spencer, J. (2007) Structural basis for the role of Asp-120 in metallo-β-lactamases. *Biochemistry 46*, 10664−10674.
(60) Yamaguchi, Y., Kuroki, T., Yasuzawa, H., Higashi, T., Jin, W., Kawanami, A., Yamagata, Y., Arakawa, Y., Goto, M., and Kurosaki, H. (2005) Probing the role of Asp-120(81) of metallo-β-lactamase (IMP-1) by site-directed mutagenesis, kinetic studies, and X-ray crystallography. *J. Biol. Chem. 280*, 20824−20832.
(61) Park, H., Brothers, E. N., and Merz, K. M. Jr. (2005) Hybrid QM/MM and DFT investigations of the catalytic mechanism and inhibition of the dinuclear zinc metallo-β-lactamase CcrA from *Bacteroides fragilis*. *J. Am. Chem. Soc. 127*, 4232−4241.
(62) Garrity, J. D., Carenbauer, A. L., Herron, L. R., and Crowder, M. W. (2004) Metal binding Asp-120 in metallo-β-lactamase L1 from *Stenotrophomonas maltophilia* plays a crucial role in catalysis. *J. Biol. Chem. 279*, 920−927.
(63) Llarrull, L.I., Fabiane, S. M., Kowalski, J. M., Bennett, B., Sutton, B. J., and Vila, A. J. (2007) Asp-120 locates Zn2 for optimal metallo-β-lactamase activity. *J. Biol. Chem. 282*, 18276−18285.
(64) Rasia, R. M., and Vila, A. J. (2002) Exploring the role and the binding affinity of a second zinc equivalent in *B. cereus* metallo-β-lactamase. *Biochemistry 41*, 1853−1860.
(65) Xu, D., Guo, G., and Cui, Q. (2007) Antibiotic deactivation by a dizinc β-lactamase: Mechanistic insights from QM/MM and DFT studies. *J. Am. Chem. Soc. 129*, 10814−10822.
(66) Badarau, A., and Page, M. I. (2006) The variation of catalytic efficiency of *Bacillus cereus* metallo-β-lactamase with different active site metal ions. *Biochemistry 45*, 10654−10666.
(67) Davies, A. M., Rasia, R. M., Vila, A. J., Sutton, B. J., and Fabiane, S. M. (2005) Effect of pH on the active site of an Arg121Cys mutant of the metallo-β-lactamase from *Bacillus cereus*: Implications for the enzyme mechanism. *Biochemistry 44*, 4841−4849.
(68) Schilling, O., Vogel, A., Kostelecky, B., Natal da Luz, H., Spemann, D., Spath, B., Marchfelder, A., Troger, W., and Meyer-Klaucke, W. (2005) Zinc- and iron-dependent cytosolic metallo-β-lactamase domain proteins exhibit similar zinc-binding affinities, independent of an atypical glutamate at the metal-binding site. *Biochem. J. 385*, 145−153.
(69) Spath, B., Settele, F., Schilling, O., D'Angelo, I., Vogel, A., Feldmann, I., Meyer-Klaucke, W., and Marchfelder, A. (2007) Metal requirements and phosphodiesterase activity of tRNase Z enzymes. *Biochemistry 46*, 14742−14750.
(70) Tomatis, P. E., Rasia, R. M., Segovia, L., and Vila, A. J. (2005) Mimicking natural evolution in metallo-β-lactamases through second-shell ligand mutations. *Proc. Natl. Acad. Sci. U.S.A. 102*, 13761−13766.
(71) Wommer, S., Rival, S., Heinz, U., Galleni, M., Frere, J. M., Franceschini, N., Amicosante, G., Rasmussen, B., Bauer, R., and Adolph, H. W. (2002) Substrate-activated zinc binding of metallo-β-lactamases: Physiological importance of mononuclear enzymes. *J. Biol. Chem. 277*, 24142−24147.
(72) Heinz, U., and Adolph, H. W. (2004) Metallo-β-lactamases: Two binding sites for one catalytic metal ion? *Cell. Mol. Life Sci. 61*, 2827−2839.
(73) Abriata, L. A., Gonzalez, L. J., Llarrull, L. I., Tomatis, P. E., Myers, W. K., Costello, A. L., Tierney, D. L., and Vila, A. J. (2008) Engineered mononuclear variants in *Bacillus cereus* metallo-β-lactamase BcII are inactive. *Biochemistry 47*, 8590−8599.
(74) Patzer, S. I., and Hantke, K. (2001) Dual repression by Fe^{2+}-Fur and Mn^{2+}-MntR of the *mntH* gene, encoding an NRAMP-like Mn^{2+} transporter in *Escherichia coli*. *J. Bacteriol. 183*, 4806−4813.
(75) Kehres, D. G., and Maguire, M. E. (2003) Emerging themes in manganese transport, biochemistry and pathogenesis in bacteria. *FEMS Microbiol. Rev. 27*, 263−290.
(76) Spath, B., Schubert, S., Lieberoth, A., Settele, F., Schutz, S., Fischer, S., and Marchfelder, A. (2008) Two archaeal tRNase Z enzymes: Similar but different. *Arch. Microbiol. 190*, 301−308.
(77) Wenzel, N. F., Carenbauer, A. L., Pfiester, M. P., Schilling, O., Meyer-Klaucke, W., Makaroff, C. A., and Crowder, M. W. (2004) The binding of iron and zinc to glyoxalase II occurs exclusively as di-metal centers and is unique within the metallo-β-lactamase family. *J. Biol. Inorg. Chem. 9*, 429−438.
(78) Nikolic-Hughes, I., Rees, D. C., and Herschlag, D. (2004) Do electrostatic interactions with positively charged active site groups tighten the transition state for enzymatic phosphoryl transfer? *J. Am. Chem. Soc. 126*, 11814−11819.